https://doi.org/10.1016/j.jmbbm.2021.104713

1. **Title page: Comprehensive computational analysis of the crimping procedure of PLLA BVS: effects of material viscous-plastic and temperature dependent behavior**

Luca Antonini[1], Gianluca Poletti[1], Lorenzo Mandelli[1], Gabriele Dubini[1], Giancarlo Pennati[1], Lorenza Petrini[2,Δ]

[1] Laboratory of Biological Structure Mechanics, Department of Chemistry, Materials and Chemical Engineering “Giulio Natta”, Politecnico di Milano, Piazza Leonardo da Vinci 32, 20133 Milano (Italy)
[2] Department of Civil and Environmental Engineering, Politecnico di Milano, Piazza Leonardo da Vinci 32, 20133 Milano (Italy)

Author email address:
Luca Antonini: luca.antonini@polimi.it
Gianluca Poletti: gianluca.poletti@mail.polimi.it
Lorenzo Mandelli: lorenzo.mandelli@polimi.it
Gabriele Dubini: gabriele.dubini@polimi.it
Giancarlo Pennati: giancarlo.pennati@polimi.it
Lorenza Petrini: lorenza.petrini@polimi.it

Corresponding Author:
[Δ] Lorenza Petrini, Tel.: +39 02 2399 4307; fax: +39 02 2399 4286.

Conflict of interest
None.

2. Abstract and key terms

Recently, researchers focused their attention on the use of polymeric bioresorbable vascular scaffolds (BVSs) as alternative to permanent metallic drug-eluting stents (DESs) for the treatment of atherosclerotic coronary arteries. Due to the different mechanical properties, polymeric stents, if compared to DESs, are characterized by larger strut size and specific design. It implies that during the crimping phase, BVSs undergo higher deformation and the packing of the struts, making this process potentially critical for the onset of damage. In this work, a computational study on the crimping procedure of a PLLA stent, inspired by the Absorb GT1 (Abbott Vascular) design, is performed, with the aim of evaluating how different strategies (loading steps, velocities and temperatures) can influence the results in terms of damage risk and final crimped diameter. For these simulations, an elastic-viscous-plastic model was adopted, based on experimental results, obtained from tensile testing of PLLA specimens loaded according to ad hoc experimental protocols. Furthermore, the results of these simulations were compared with those obtained by neglecting strain rate and temperature dependence in the material model (as often done in the literature), showing how this lead to significant differences in the prediction of the crimped diameter and internal stress state.

Coronary stent; strain rate dependent materials; polymeric materials; experimental characterization; material calibration; in-silico model.

3. Introduction

The main treatment of coronary artery stenosis consists of percutaneous coronary intervention (PCI), a minimally invasive surgical procedure involving the deployment of a stent which restores the physiological lumen of the occluded vessel (Blair et al., 2019; Debusschere et al., 2015). Generally, implanted devices are bare-metal stents (BMSs) and drug-eluting stents (DESs), made of different types of metal alloys and intended to remain permanently within the artery. The permanent presence of the device has some well-known side effects, first of all, in-stent restenosis and the risk of thrombosis, related with an inflammation of the artery walls and disorders to regular blood flow dynamics (Bobel and McHugh, 2018; Debusschere et al., 2015; Soares et al., 2010). For these reasons, research today has focused its attention on devices that support the walls of the vessel only in the initial phase of the healing process and that are reabsorbed when their action is no longer required: bioresorbable vascular scaffolds (BVSs). To maintain the vessel lumen pervious at the time of implantation, the radial stiffness of BVSs must therefore be comparable to that guaranteed by BMSs and DESs. For this reason, it is essential to choose a biodegradable material having adequate mechanical properties and also suitable degradation times for application in coronary arteries. Both polymers and metals, such as magnesium or iron alloy, can have the mentioned characteristics. Among the polymers, the poly-L-lactic-acid (PLLA) has recently established itself as valid material for the manufacture of BVSs (Bergström and Hayman, 2016; Muliana and Rajagopal, 2012; Pauck and Reddy, 2015). If coupled with an appropriate size of the stent struts, it ensures enough radial stiffness and has a sufficiently long degradation period to support the vessel in the early stages of the healing process (Bobel et al., 2015). Compared to common metal alloys generally used for the manufacture of BMSs or DESs, the PLLA is much more complex and can be challenging to model due to the high non-linearity of its mechanical behavior (Bergström and Hayman, 2016; Bobel et al., 2015; Muliana and Rajagopal, 2012). In particular, this characteristic is mainly due to the proximity of the glass transition temperature (about 60°C) with the operating temperatures of the coronary stents (about 50°C during the crimping phase, room temperature at the time of surgery, and 37°C when implanted in the patient). The material mechanical behavior is highly dependent on the working temperature and the deformation rate. The latter plays a significant role when the material exceeds the yield strength and enters the plastic field, thus exhibiting a viscous-plastic behavior (Bergström and Hayman, 2016; Bobel et al., 2015).

To evaluate the pre-clinical performance of coronary stents, it is advisable to develop a digital twin of the device which can be analysed to investigate all those quantities that would be difficult or even impossible to evaluate with in-vitro studies (e.g. local stresses and strains, the extent of plasticization, etc.) (Blair et al., 2019). The computational study of polymeric stents is a rather new topic and the literature dealing with this subject is relatively limited compared to what has been produced regarding conventional metal stents (T. Y. Qiu et al., 2018; Schiavone et al., 2016). Among them, Pauck and Reddy (2015) demonstrated through finite element analysis how the radial stiffness of PLLA stents of different designs was closely related to the stent-specific

geometric dimensions and mechanical properties of the material that was modelled as anisotropic elastic-plastic. With a descriptive model of the PLLA that takes into account the viscous behavior of the polymer derived from the literature works by Bergstrom et al. (2002) and Eswaran et al. (2011), Debuscherre et al. (2015) used an implicit finite element solver demonstrating that the application of a step-wise procedure for balloon inflation reduces the occurrence of high stress values in the fully expanded Absorb stent (Abbot Vascular, USA). Adopting a PLLA model with elastic-plastic and non-linear hardening characteristics, Schiavone et al. (2016) compared the performance of the Absorb stent with the Xience V stent (MultiLink Vision platform design, Abbot Vascular, USA), made of Co-Cr L605, when implanted in pathological arteries with symmetrical and eccentric plaques. Qiu et al. (2018), again using the material model proposed by Pauck and Reddy (2015) for the PLLA, simulated the crimping and expansion process of four polymeric stents (Absorb, Elixir, Igaki-Tamai, and Reva Medical) intending to carry out a comparative study in terms of stress values achieved, pressure-diameter relationship, elastic recoil, and radial stiffness. A computational study using a material model that takes into account the non-linearities of the PLLA is the one proposed by Bobel and McHugh (2018). In this work, the PLLA has been described through a Parallel Rheological Framework (PRF) composed of hyperelastic, viscoelastic, and plastic (isotropic hardening) elements and it has been investigated how a shape memory effect (SME) can improve the performance in terms of recoil on the polymeric stent Absorb.

As can be seen from this brief review of the literature on the computational studies of PLLA stents, although the non-linearities of the behavior of this polymer are well known, there is generally a tendency to neglect the dependence on temperature or deformation rate in favour of a simpler and easier to implement model. This is justifiable when simulations aim to guide the pre-operative planning and attention is focused on stent expansion: in-silico analyses of stent deployment in patient-specific arteries are used to estimate the procedure efficacy, namely the reopening of the vessel lumen. On the contrary, in the design phase, it is fundamental to have a tool able to provide specific information on the device, as the local stress state, to assess the risk of failure starting from the analysis of the first procedural step in which the device is stressed, i.e. the crimping phase. Compared to DES and BMS, polymeric BVS are subjected to greater deformation during the crimping phase. Their struts are indeed larger. Besides, the polymeric stents are obtained by laser cutting from a tube with a diameter equal to that of the fully expanded stent, while, for metal stents, tubes of intermediate dimensions between the diameter of the crimped and expanded configurations are used. These high levels of deformation could cause damages to the stent struts and a subsequent change in mechanical properties and degradation process of the material (Wang et al., 2020). Moreover, during the crimping phase, the speed used to perform the procedure and the operating temperature affect the stress distribution in the stent and hence the risk of damage (Bobel and McHugh, 2018; Cabrera et al., 2017; Jow et al., 2012). A numerical model able to correctly describe the stent behavior during crimping would allow a better design of the crimping procedure.

This work carries out a computational study of the crimping procedure of PLLA BVS

on a stent unit inspired by the geometry of the Absorb GT1 stent (Abbott Vascular, USA). Special care is taken to characterize and model the viscous-plastic behavior and the temperature dependence of the PLLA, starting from experimental tests performed on dog-bone material specimens. The purpose is to investigate through numerical simulations different strategies for the crimping procedure, observing how the temperature and the duration of the procedure can be optimized to avoid the onset of stress and deformations potentially dangerous for the integrity of the device.

4. Materials and methods

4.1 Experimental campaign

For this study, six PLLA dog-bone samples obtained by laser cutting from the same tubes used for PLLA stents manufacturing were available. Table 1 shows the dimensions of the specimens.

Table 1 - PLLA dog-bone samples: geometrical dimensions.

	Value [mm]
Gauge length, L_0	5.00
Width, W_0	2.00
Thickness, t	0.115

The tests were carried out at three different temperatures, corresponding to the common working conditions: at room temperature (25°C), inside the human body (37°C) and 15°C below the glass transition (52°C), temperature inspired by those used during the crimping procedure (Jow et al., 2012). For each temperature two deformation rates, 0.1%/s and 10%/s, were investigated. The experimental protocol was set to optimize the information that could be extracted from the tests since only a limited number of samples were available. Therefore, it was chosen to perform longitudinal tensile tests with the loading phase interspersed with a relaxation step. The relaxation step allowed to characterize the material even in a quasi-static regime. In fact, during crimping and expansion, the stent struts are subject to bending, with a linear distribution of strain along the cross-section. Accordingly, the PLLA is subjected to a strain rate varying from zero up to a maximum value, depending on the global speed of the external load. The experimental protocol consisted of three steps:

- *Tensile Load 1*: the sample is stretched up to 1.5 mm (≈ 26% of true strain);
- *Displacement Maintenance*: the reached displacement is maintained for 1800 s to allow the stress relaxation;
- *Tensile Load 2*: the sample is stretched up to 5.0 mm (≈ 70% of true strain).

The tests were performed in displacement-controlled mode and were carried out using the BOSE Enduratec ELF 3200 mono-axial testing machine, mounted with a 200 N

load cell and coupled with a removable oven, used to set and control the test temperature. For each specimen, force and displacement signals were registered by the machine.

4.2 Material calibration

Based on the obtained results (in agreement with PLLA experimental analyses reported in the literature (Bobel and McHugh, 2018)), an elastic-viscous-plastic (VP) material model, dependent on the temperature, was chosen. In particular, the purely empirical Johnson-Cook model, available in the commercial code ABAQUS (Dassault Systems Simulia Corp., Johnston, RI, USA) was used to describe the viscous-plastic behavior with isotropic hardening, through the following equation:

$$\bar{\sigma}_{pl} = \left[A + B\left(\bar{\varepsilon}_{pl}\right)^{n}\right]\left[1 + C \cdot ln\left(\frac{\dot{\bar{\varepsilon}}_{pl}}{\dot{\varepsilon}_0}\right)\right]$$

where:

- $\bar{\sigma}_{pl}$ is the equivalent plastic stress;
- $\bar{\varepsilon}_{pl}$ is the equivalent plastic strain;
- A is the first yield stress (when $\bar{\varepsilon}_{pl} = 0$) under quasi-static condition;
- B is the strain hardening constant;
- n is the strain hardening coefficient;
- $\dot{\bar{\varepsilon}}_{pl}$ is the equivalent plastic strain rate;
- $\dot{\varepsilon}_0$ is the reference strain rate associated with the quasi-static curve;
- C is the strain rate constant.

Accordingly to the above equation, the parameters to be identified for using the material model are seven: Young's Modulus (E) and the Poisson's Ratio (ν) for the elastic field, A, B, C, n, and $\dot{\varepsilon}_0$ for the viscous-plastic part. These parameters were calibrated based on experimental results for each of the three considered temperatures.

Regarding the elastic parameters, the Young's Modulus (E) was estimated as the average value of those obtained at the two test speeds. The Poisson's Ratio (ν), on the other hand, was chosen based on literature. Despite it ranges from the values commonly associated with metallic materials, $\nu = 0.3$, (T. Y. Qiu et al., 2018; Schiavone et al., 2016; Wang et al., 2017) up to a maximum of $\nu = 0.46$, (Bergström et al., 2002) the present work relies on studies in which $\nu = 0.45$ (Bobel et al., 2015; Muliana and Rajagopal, 2012).

The calibration of the viscous-plastic parameters was carried out in two phases. In the first phase, a preliminary evaluation was performed using the analytical formulation of the Johnson-Cook model and the Microsoft Excel solver tool based on the Generalized Reduced Gradient method. From the experimental force-displacement curves converted into stress-strain curves, the parts related to plastic behavior during the loading steps, disregarding the relaxation phase, were extracted. In this way, for the

two test speeds at each temperature, a continuous experimental stress-plastic strain relationship was obtained and compared with the analytical one. The viscous-plastic parameters were optimized minimizing the difference between experimental and analytical data. The evaluation of the quasi-static behavior was made considering the stress-relaxation step and assuming that, for each temperature, the point corresponding to the minimum stress value (i.e. that reached at the end of the relaxation phase) belongs to the quasi-static curve of the material: hence, the static stress-plastic strain curve was enforced to pass through that point. The parameters found with the analytical formulation were used to reproduce in-silico the experimental tests on dog-bone samples. A virtual model of the specimen was developed, based on its actual size, and meshed with hexahedral elements with reduced integration (C3D8R). Given the symmetry of the specimen, simulations were performed on a quarter of the real geometry, imposing appropriate constraints and symmetry conditions to faithfully replicate the experimental environment. Differently from what was done with Excel, in this case, the whole experimental protocol was reproduced, to obtain a numerical comparison also for the stress-relaxation phase in terms of force-time curves. The results showed a mismatch between experimental and numerical curves for large displacements, requiring a second calibration step. Coupling finite element analyses and manual tuning of material parameters, three different viscous-plastic PLLA models have been developed, able to replicate the mechanical behavior of the real material at 25°C, 37°C, and 52°C, hereinafter referred to as 25_VP, 37_VP, and 52_VP, where the first number indicates the testing temperature and VP stands for elastic-viscous-plastic.

Moreover, for comparison purposes, it was also decided to build a simple elastic-plastic material model (disregarding viscous effects) for describing the mechanical response of PLLA. Based on the six experimental stress-strain curves (three temperatures and two velocities), six elastic-plastic material models were calibrated, labelled as follows: 25_EP_01, 25_EP_10, 37_EP_01, 37_EP_10, 52_EP_01 and 52_EP_10, where the first number indicates the testing temperature, EP stands for elastic-plastic and the final number refers to the test speed adopted as reference. These models were used to perform the crimping analysis.

4.3 Numerical analysis of the stent crimping procedure

After production by laser cutting from the manufacturing tube, crimping is the first step inducing deformations on the stent. The purpose of this procedure is indeed to reach a reduced diameter configuration that allows the coupling with the folded expandable balloon and hence the insertion into the catheter, obtaining the so called “delivery system”. Given that such delivery system needs to be inserted into the lumen of a stenotic vessel, smaller crimped diameters are to be preferred. During crimping phase, the diameter is forced to about 40% of the initial value and the struts are packed one against the other, with large areas of contact. This procedure is performed using a crimping machine, consisting of rigid planes arranged circumferentially that move

radially to crimp the stent above the balloon and then reopen. Accordingly, the stent diameter reaches a minimum at the end of the planes closing phase and slightly increases when planes reopen, due to elastic and viscous effects. For BVS stents, each manufacturer has developed its procedure, aiming to achieve the best compromise between the small diameter of the crimped device and the risk of damage related to the high strain induced in the device. Usually, the process is divided into several phases in which the crimping machine alternates between diameter reduction and maintenance steps and in which the balloon is pressurized (Jow et al., 2012). Temperature and velocity affect the material response. Therefore, having a computational model able to predict the solicitations induced into the stent during the specific crimping procedure may be useful for the design of a safer and more effective procedure. In this context, several simulations of crimping procedures have been performed, differing for the adopted strategy. In such numerical analysis, the PLLA was described through the developed material models. This activity has the dual purpose of investigating how different crimping methods may affect stent performance and verifying which modelling strategies are reliable for such an analysis.

4.3.1 Crimping simulations with different materials

Although it is known that the crimping procedures of polymeric stents are generally complex (Jow et al., 2012), in the literature (Bobel et al., 2015; Debusschere et al., 2015; T. Qiu et al., 2018; T. Y. Qiu et al., 2018) those who perform computational analysis on PLLA BVSs tend to simplify the process focusing the attention only on the expansion phase or on other post-expansion tests. Moreover, as already stated, generally in numerical simulations the viscous effects of the material or its dependence on the operating temperature are neglected, describing the PLLA with material model parameters suitable for the behavior at 37°C (to be consistent with the temperature reached once implanted inside the human body).
To evaluate the limits of such model simplifications, the non-viscous and viscous PLLA models previously described were employed to simulate a simplified crimping procedure (hereinafter named PS), consisting of two steps: a machine planes closing step, and a reopening step. For the simulations in which the strain rate-sensitive material models were used, the crimping procedure was applied at two different speeds: in one, the action of closing the planes lasted 30 s and in the other 150 s, both the reopening step lasted 1 s. These two protocols are hereinafter labelled as PS_{30} and PS_{150}. The simulation results were compared in terms of the radial force exerted by the device on the crimping planes, the diameter reached by the stent at the end of the simulation (after planes reopening), the elastic recoil (i.e. the percentage of diameter re-opening compared to the minimum value reached during the crimping phase), and the internal stresses in the device (indicative of potential damages).

4.3.2 Crimping simulations with different procedures

Concentrating the attention on the viscous-plastic models, a further set of simulations

was performed to explore the freedom of choice in the definition of the crimping procedure by manufacturing companies. Compared to the deployment phase in which time and temperature constraints are dictated by the needs of the clinical act, the crimping procedure can be adapted to safeguard the integrity of the BVS by acting on the duration of the different steps of the procedure and the operating temperature. In particular, seen experimentally the ability of the polymer to relax the stress by keeping the deformation fixed, three procedures were set differing in the duration of the crimping step (15 s, 30 s, and 60 s), followed by a 30 s holding step and a 1 s reopening step: they will be hereinafter labelled as PH_{15}, PH_{30}, and PH_{60}. Each of these procedures was coupled with the three viscous PLLA material models, namely 25_VP, 37_VP, and 52_VP.

Finally, the viscous model was exploited also by performing two complex crimping simulations inspired by the instructions for crimping polymeric stents, that foresee different steps of crimping and holding, and the possibility of partially inflating the balloon to avoid stent strut distortion during the phase of diameter reduction. In particular, in the first one, the crimping protocol described in the patent by Jow et al. (2012) was replicated. The simulation was organized in the following steps:

- *Crimping 1* (10 s): stent outer diameter was reduced up to 2.11 mm;
- *Holding 1* (30 s): the diameter was maintained at the reached position to allow the stress relaxation of the PLLA;
- *Crimping 2* (10 s): the external diameter was reduced up to 1.73 mm while the balloon was inflated at 1.16 atm;
- *Holding 2* (15 s): both the pressure within the balloon and external diameter were maintained during this step;
- *Crimping 3* (10 s): the pressure inside the balloon was released and the external diameter of the stent was reduced up to 1.19 mm;
- *Holding 3* (200 s): the reached configuration was maintained allowing the stress relaxation;
- *Release* (1 s): the elastic recoil of the device was allowed.

The second simulation used a procedure similar to the one described above: same division of the various steps and same deformation rate of the stent, but different minimum diameter reached before the *Holding 3* step. In this case, during the *Crimping 3* step, the stent was crimped up to 1.09 mm in 12 s (the difference in step time is intended to use the same speed of the crimping planes adopted by the patent protocol). The aim was to check whether or not a small variation (0.1 mm) in the final crimping diameter may affects the recoil and the risk of potential damage to the structure of the BVS. The first protocol, because inspired by the patent, is hereinafter labelled as PP, while the second as Modified_PP. According to the indications that the device is heated to high temperatures during the real procedure, in the two simulations, the material model reflecting the viscous behavior of the PLLA at 52°C was used.

4.3.3 Development of the finite element model

A coronary stent inspired by the design of Absorb GT1 with 3.00 mm diameter (Abbot Vascular) was considered. The information necessary for the development of the finite element model was derived from the detailed description of the design released in the FDA Executive Summary of the Absorb GT1. To keep the computational cost low, the CAD of a 3D geometry, considering only a portion of the stent (Figure 1a), i.e. three rings (two ends connected by a central unit) was built using SolidWorks software (Dassault Systèmes SolidWorks Corp. Waltham, MA, USA). The mesh generation was performed using Altair HyperMesh software (Altair Engineering Inc., Troy, MI, USA). The initial partitioning of the surface geometry allowed the development of an extremely smooth and regular mesh pattern (Figure 1a inset). Reduced integration hexahedral elements (C3D8R) were chosen for this study.
The action of the crimping machine was replicated in-silico with sixteen rigid planes arranged circumferentially around the stent with imposed radial displacement. The planes were modelled as discrete rigid parts and meshed with R3D4 elements. The balloon, used in the simulations of PP and Modified_PP, was described with a simplified model consisting of membrane elements M3D4, based on previous literature(Morris et al., 2018). In Figure 1b the crimping planes positioned around the stent and the balloon are shown.
For all the numerical analysis, an explicit solver (ABAQUS/Explicit), able to manage solidly and robustly the contacts that take place during crimping, was preferred to the implicit approach, also in accordance with numerous literature works (Bobel and McHugh, 2018; T. Qiu et al., 2018; T. Y. Qiu et al., 2018; Schiavone et al., 2017).

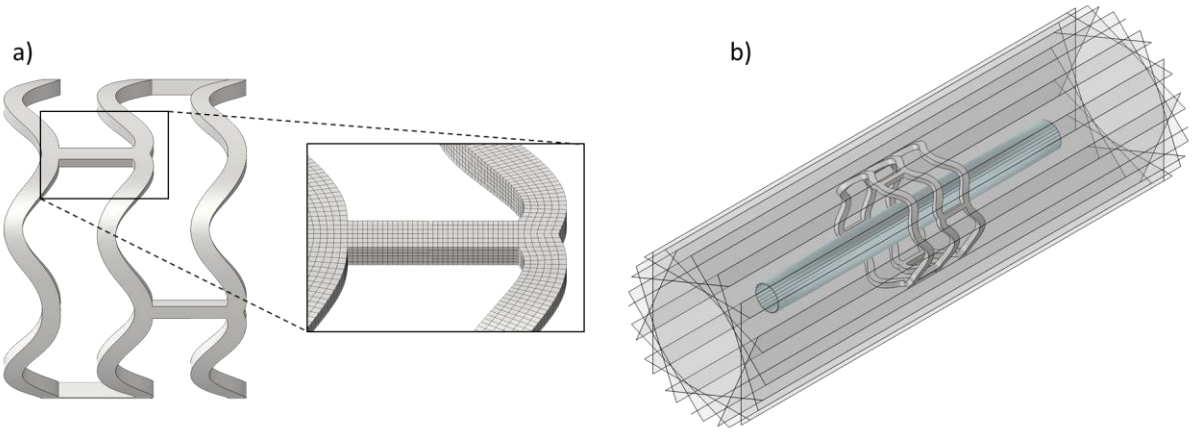

Figure 1 - a) 3D model of the stent unit inspired by the Absorb GT1 design with detail of a meshed strut (in the inset); b) initial configuration of the crimping simulation with the crimping planes positioned circumferentially to the stent and balloon.

5. Results

5.1 Experimental campaign

The results of the experimental tests on PLLA samples are shown in Figure 2 (left side) in terms of force-displacement curves. As expected, a stiffer and more brittle material response was observed as temperature decreases and the strain rate increases. The

normalized force trend over relaxation time (Figure 2, right side) highlights a significant dependence on strain rate and temperature also in the stress relaxation quantity. To calibrate the material model analytically, the experimental stress-strain curves were derived and reported in Figure 3.

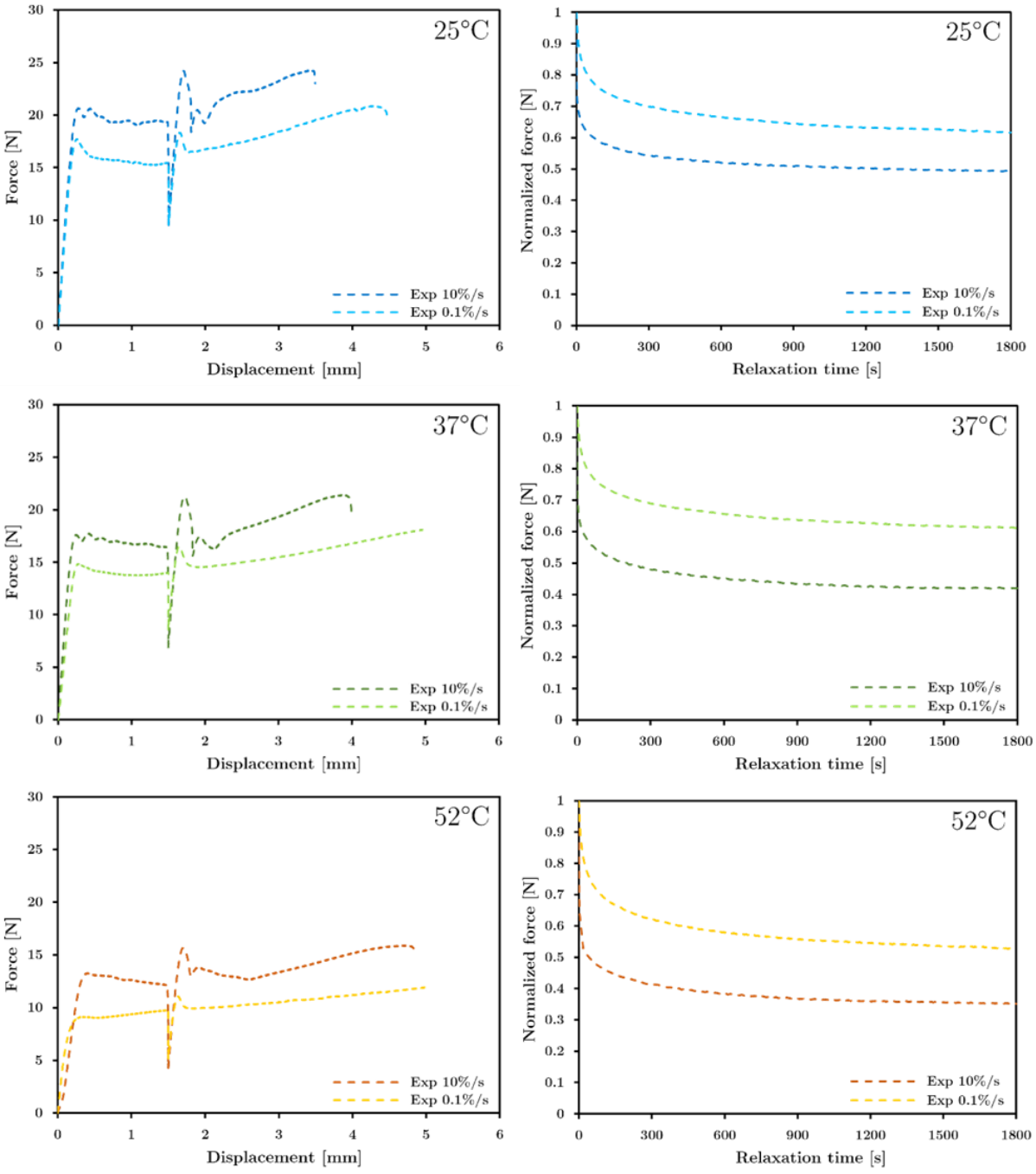

Figure 2 - Experimental results in terms of Force-Displacement curves (left side) and Normalized force-Relaxation time curves (right side) obtained at the two strain rates: 10%/s and 0.1%/s. The results are reported for each tested temperature (25°C, 37°C, and 52°C).

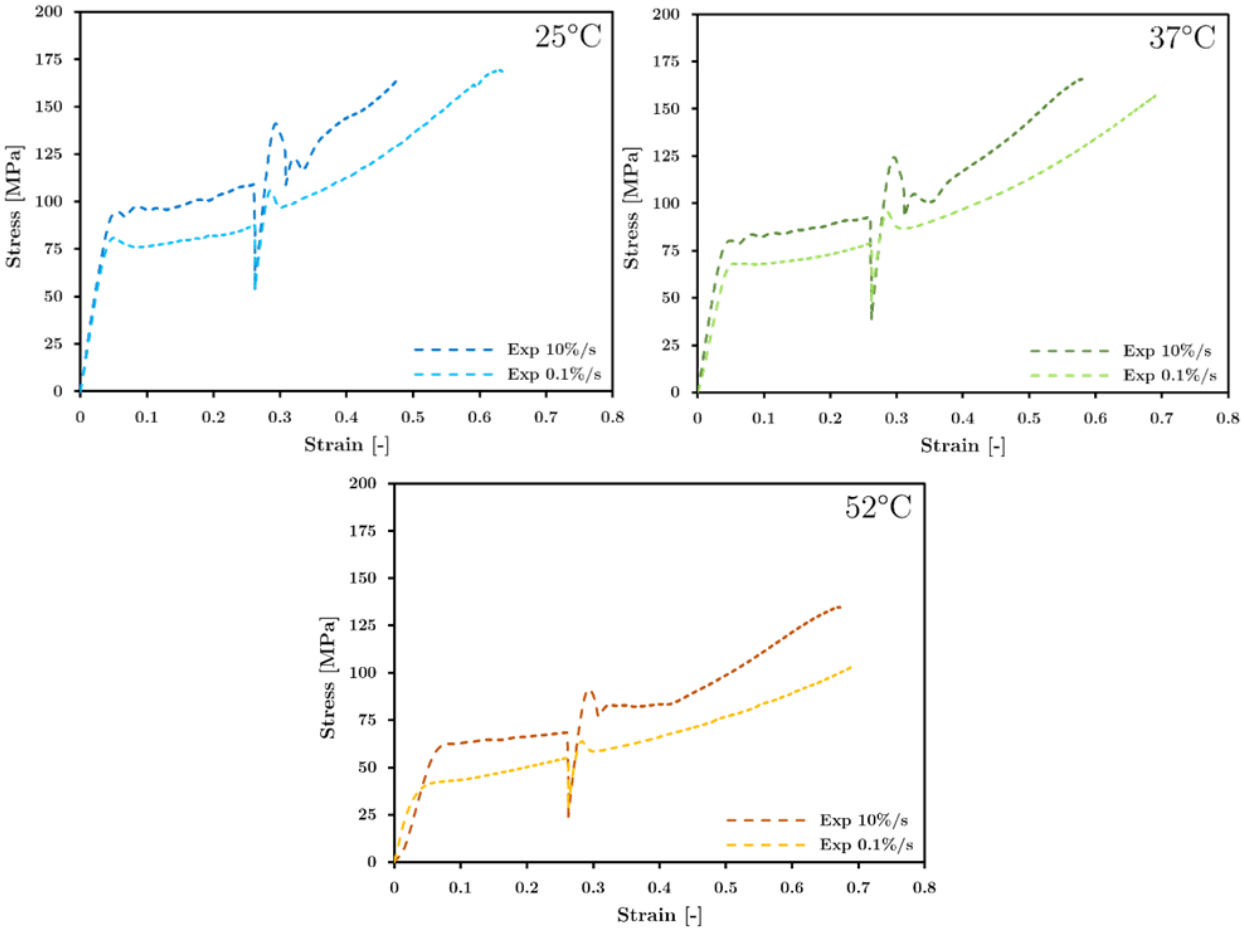

Figure 3 - Experimental results obtained at the two strain rates (10%/s and 0.1%/s) converted in terms of Stress-Strain curves. The results are reported for each tested temperature (25°C, 37°C, and 52°C).

5.2 Material calibration

The results of the preliminary material calibration on Excel are shown in Figure 4 for each temperature. The two specimens dedicated to the tensile tests at 25°C and the one tested at 37°C with 10%/s of strain rate broke before reaching the end of the tests. This highlighted how material damage is dependent on temperature and strain-rate: the higher is the test speed and the lower is the temperature, the highest is the breakage risk. Johnson-Cook's plasticity model can represent both hardening and the strain rate dependence that characterize the material's response. The numerical simulations of the whole experimental test also allowed the relaxation dynamics to be considered in the parameter identification. The final parameters of the three PLLA models corresponding to the different temperatures are shown in Table 2. The comparison with the experimental curves reported in Figure 5 in terms of both force-displacement (left side) and normalized force-relaxation time (right side) indicates a satisfactory ability of the model to describe the highlighted aspects of the material.

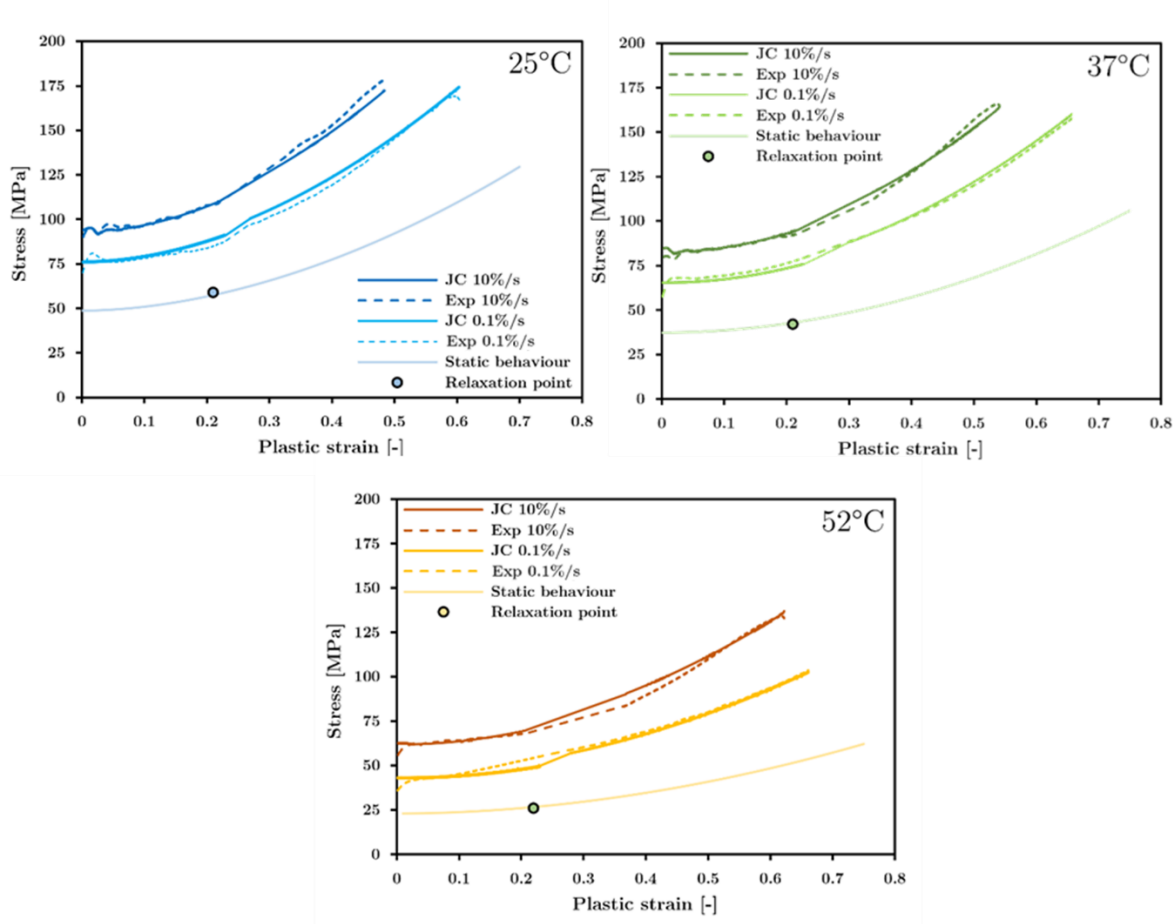

Figure 4 - Comparison between the experimental curves (Exp) and the behavior of the Johnson-Cook (JC) material model with parameters identified with Excel. The curve representing the material in quasi-static regime (Static behavior) was calibrated by imposing the intersection with the Relaxation point. The results are reported for each tested strain rate (10%/s and 0.1%/s) and temperature (25°C, 37°C, and 52°C).

Table 2 – Parameter values of the three PLLA material models (one for each temperature). For the meaning of the parameters see Section 4.2

	Elasticity model		Johnson-Cook's plasticity model				
	E (MPa)	ν (-)	A (MPa)	B (MPa)	n (-)	C (-)	$\dot{\varepsilon}_0$ (s^{-1})
25°C	2235	0.45	28	135	1.96	0.225	1.0 E-6
37°C	1850	0.45	20	90	1.97	0.295	1.0 E-6
52°C	1230	0.45	9	41	1.97	0.550	1.7 E-6

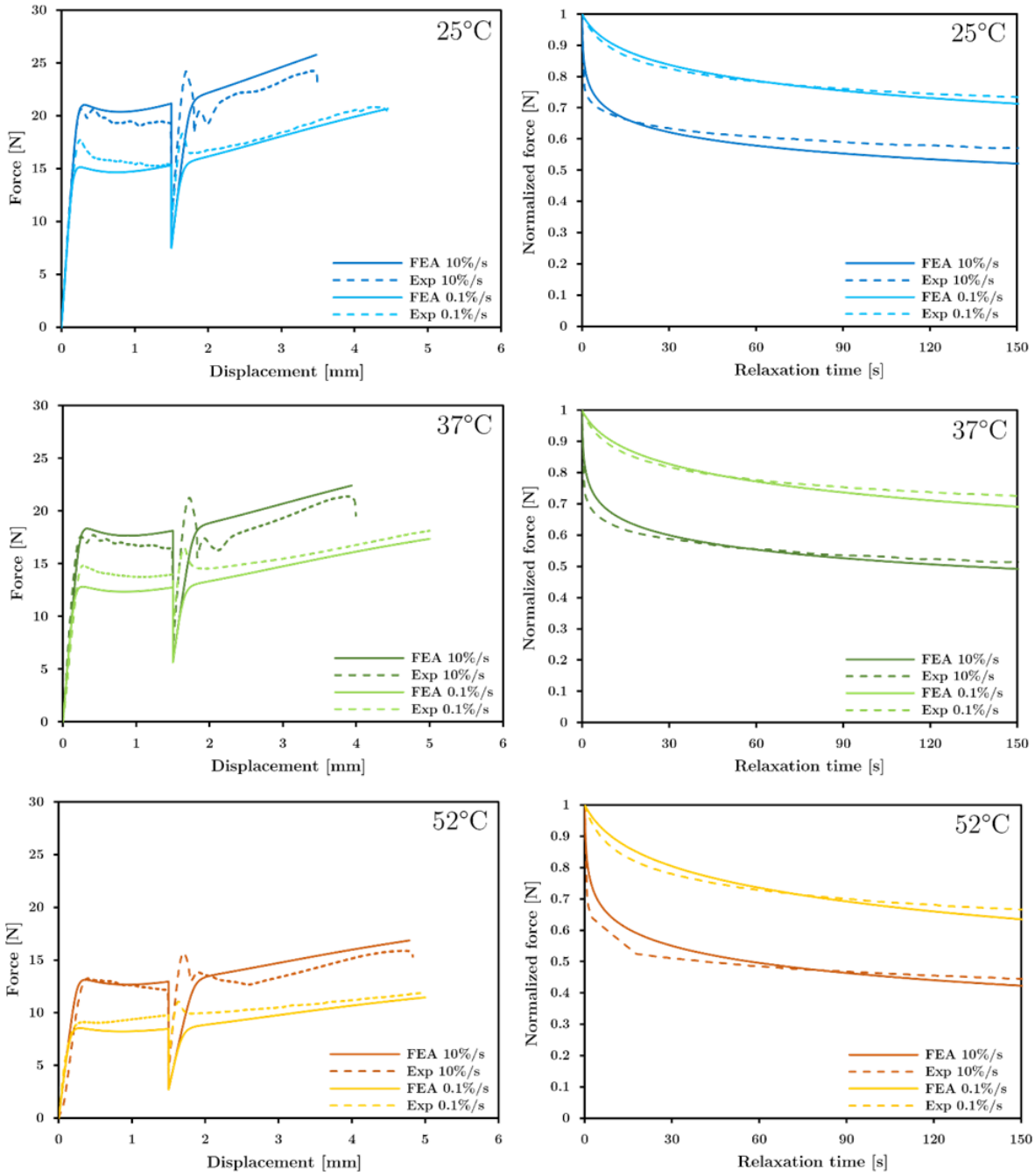

Figure 5 - Comparison between the experimental results (Exp) and the FEA's outputs (FEA) in terms of Force-Displacement curves (left side) and Normalized force-Relaxation time curves (right side). The results are reported for each tested strain rate (10%/s and 0.1%/s) and temperature (25°C, 37°C, and 52°C).

5.3 Numerical analysis of the crimping procedure

5.3.1 Crimping simulations with different materials

In Table 3 the computational results of the simplified procedure are reported in terms of external diameter reached by each stent unit and elastic recoil. As expected, lower final diameter values were obtained with material EP_01 compared to EP_10. This is because material EP_01, having been calibrated based on mechanical tests carried

out at a lower speed, reached the plastic field at lower stress values and consequently the stent plasticises more showing smaller values of elastic recoil. A similar effect, even if less evident, is due to the temperature increment. On the other hand, observing the results obtained with the viscous models, it can be seen that lower diameters are obtained when a slower crimping protocol is applied, while the temperature doesn't seem to affect so much the stent behavior.

Table 3 - External diameter and elastic recoil of the stent unit measured at the end of the simplified crimping protocol (PS) simulations, performed at three temperatures (25°C, 37°C, and 52°C), using both the elastic-plastic (EP) and elastic-viscous-plastic (VP) models.

Temperature	Simulation	External Diameter [mm]	Elastic Recoil [%]
25°C	PS_25_EP_01	1.582	32.9
	PS_25_EP_10	1.688	41.8
	PS_{30}_25_VP	1.668	40.2
	PS_{150}_25_VP	1.609	35.2
37°C	PS_37_EP_01	1.662	39.7
	PS_37_EP_10	1.711	43.8
	PS_{30}_37_VP	1.680	41.2
	PS_{150}_37_VP	1.617	35.9
52°C	PS_52_EP_01	1.616	35.8
	PS_52_EP_10	1.784	49.9
	PS_{30}_52_VP	1.682	41.3
	PS_{150}_52_VP	1.608	35.1

The results in terms of force-diameter curves are reported in Figure 6 grouped according to the operating temperature. As expected, a stiffer behavior was experienced with the elastic-plastic models calibrated considering the tensile test performed with 10%/s of strain rate, with respect to the one referring to 0.1%/s at the same temperature. Moreover, for each temperature, the elastic-viscous-plastic materials with crimping protocol PS_{30} behaved similarly to the EP_10 except for a higher peak of force at the maximum diameter reduction, while the curves obtained with the protocol PS_{150} were closer to EP_01. It is interesting to notice that there isn't a clear trend: VP models give stiffer or softer behavior compared to EP depending on the working temperature. The smallest differences are present at 37°C. Moreover, the internal state of stress in terms of Max Principal Stress was compared in Figure 7 recording the values obtained at maximum crimping, i.e. when the minimum diameter is reached (the most critical point for strut integrity). The general trend demonstrated that the lower the test temperature, the higher are the stress values. Coherently with

previous results, Figure 7 shows that the higher stress values were obtained, for the elastic-plastic cases, adopting the material models calibrated using high strain rate (10%/s) experimental test results and, for the elastic-viscous-plastic cases, using the protocol PS_{30}, inducing higher strain rate in the device.

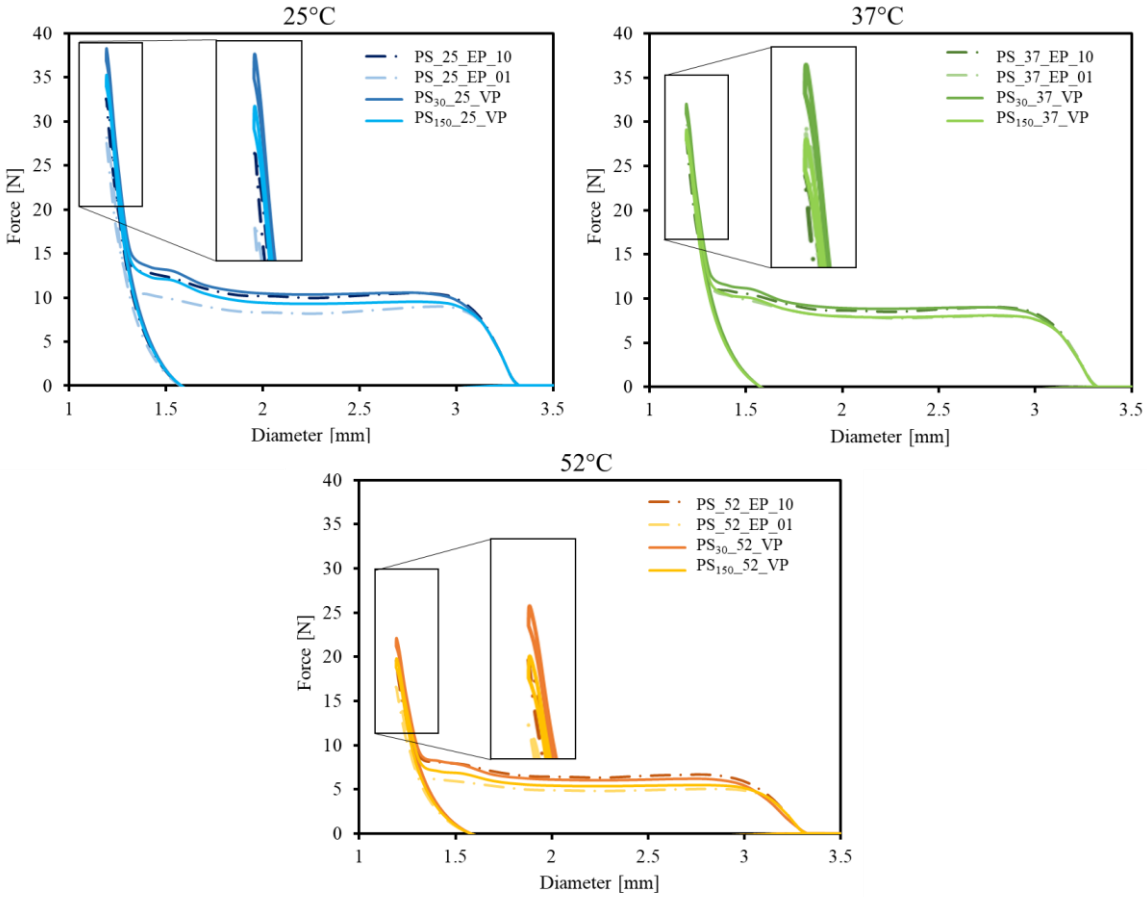

Figure 6 - Force-Diameter curves obtained simulating the simplified crimping procedure (PS) with all the developed PLLA material models, with detail of maximum force reached once the device is at the minimum diameter. The various simulations were labelled with the following strategy: the first letters refer to the crimping procedure (the presence of subscript numbers indicates a difference in step duration), then the temperature and the adopted material model are declared.

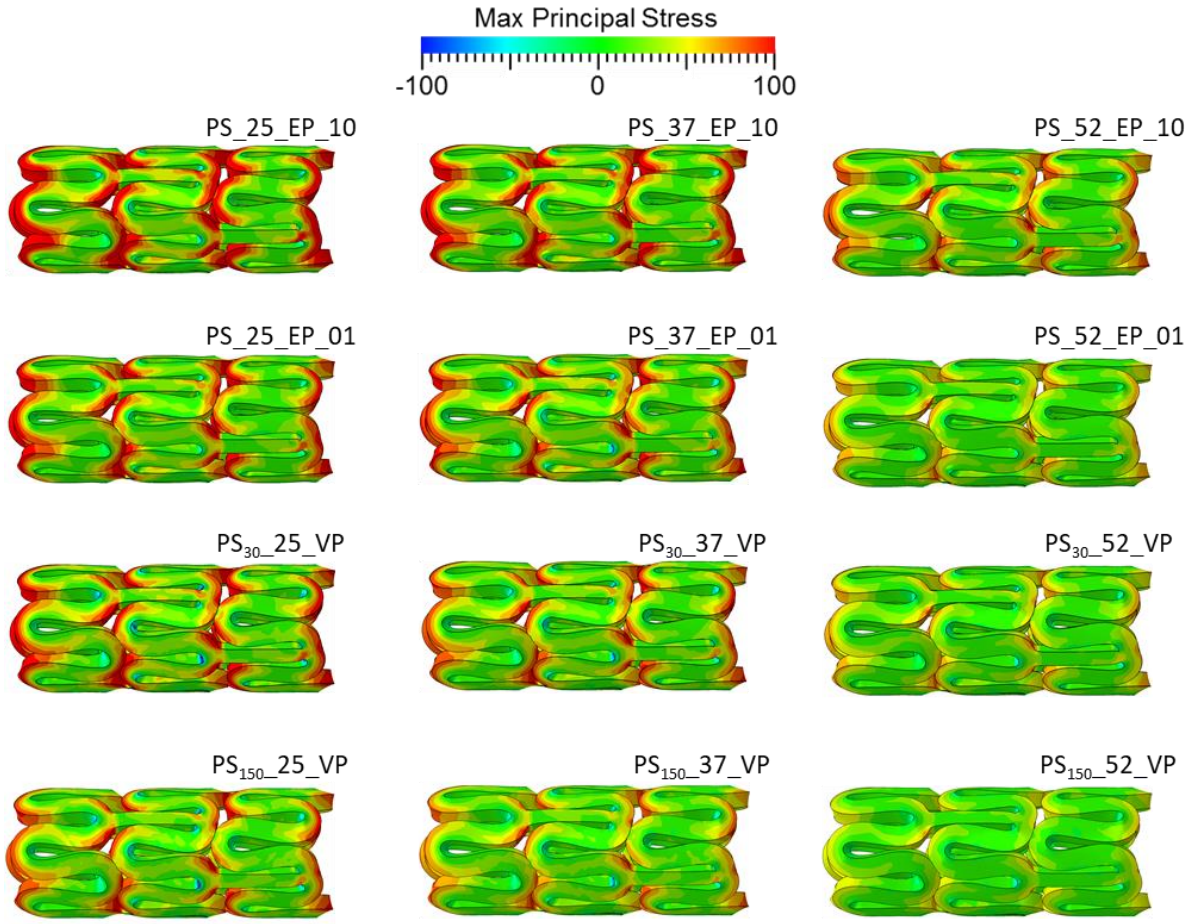

Figure 7 - Max Principal Stress recorded on the stent unit when the crimping planes reach the minimum diameter during the simplified crimping procedure for all the developed PLLA material models. The various simulations were labelled with the following strategy: the first letters refer to the crimping procedure (the presence of subscript numbers indicates a difference in step duration), then the temperature and the adopted material model are declared.

5.3.2 Crimping simulations with different procedures

The effect of including a holding phase during which the plane's position was maintained fixed to allow the stress-relaxation was observed comparing the final external diameters obtained with simulations PS_{30}_25_VP, PS_{30}_37_VP and PS_{30}_52_VP respectively with PH_{30}_25_VP, PH_{30} _37_VP and PH_{30} _52_VP. The results are reported in Table 4 and it is evident that the presence of a stress relaxation step allows the crimped stent to reach smaller diameter values, particularly the higher the temperature.

Table 4 - Comparison between the external diameters and the elastic recoils obtained at the end of the procedures, simulating crimping in 30 s followed by an immediate release of 1 s (PS_{30}) or with a holding step of 30 s between crimping and release (PH_{30}) for each elastic-viscous-plastic model.

Temperature	Crimping Procedure	External Diameter [mm]	Elastic Recoil [%]
25°C	PS_{30}	1.668	40.2

	PH_{30}	1.600	34.5
37°C	PS_{30}	1.680	41.2
	PH_{30}	1.603	34.7
52°C	PS_{30}	1.682	41.3
	PH_{30}	1.594	33.9

Also concerning the simulations with different durations of the crimping phase (PH_{15}, PH_{30} and PH_{60}), the results were compared in terms of external diameter reached at the end of the procedure and elastic recoil (Table 5), force-diameter curves (Figure 8) and stress state recorded when the minimum diameter value was reached during crimping (Figure 9). Although there were no significant differences in the external diameters and elastic recoils, more critical stress states were observed by reducing the temperature and duration of crimping protocols.

Table 5 - External diameter and elastic recoil of the stent unit measure at the end of the crimping procedures with different crimping speeds (PH_{15}, PH_{30}, and PH_{60}) for each elastic-viscous-plastic model.

Temperature	Crimping Procedure	External Diameter [mm]	Elastic Recoil [%]
25°C	PH_{15}	1.601	34.5
	PH_{30}	1.600	34.5
	PH_{60}	1.593	33.9
37°C	PH_{15}	1.606	35.0
	PH_{30}	1.603	34.7
	PH_{60}	1.599	34.4
52°C	PH_{15}	1.594	33.9
	PH_{30}	1.594	33.9
	PH_{60}	1.586	33.3

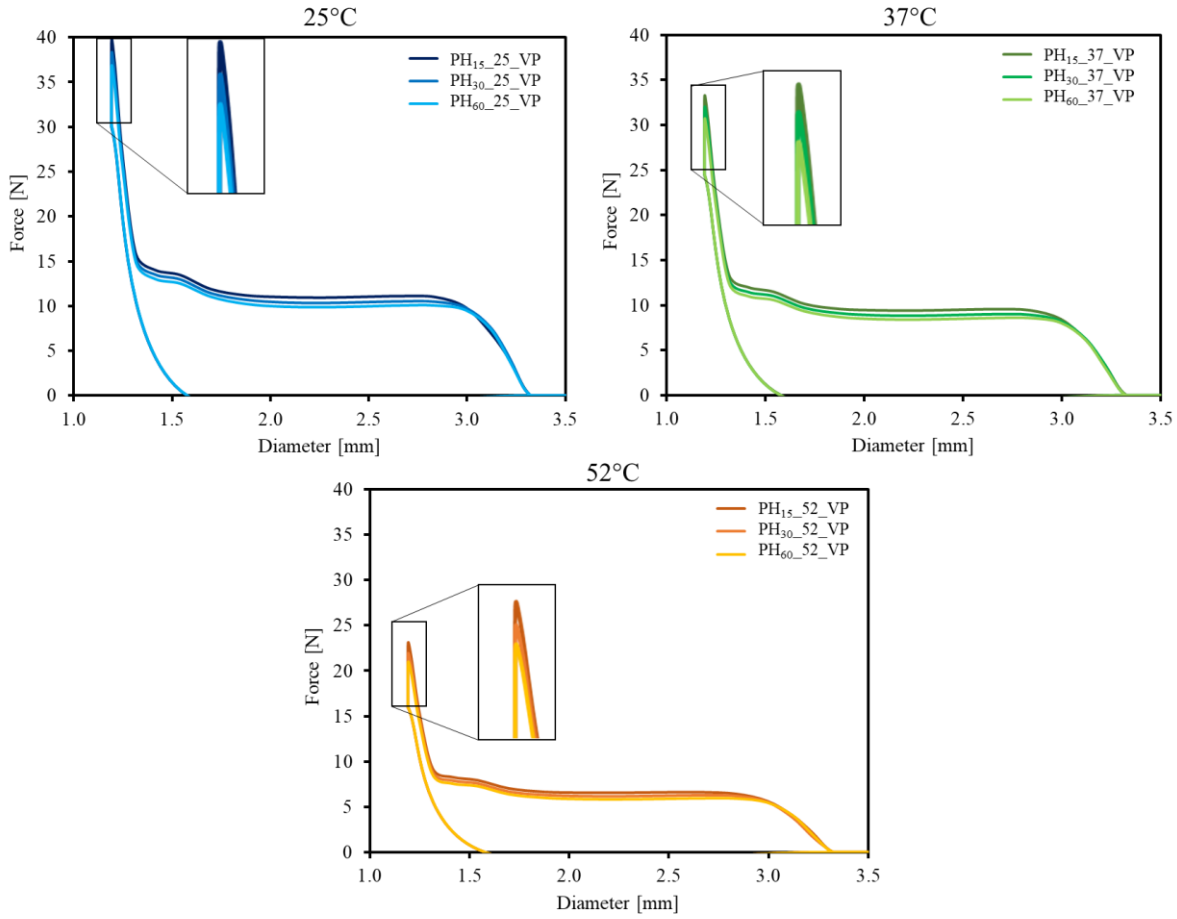

Figure 8 - Force-Diameter curves obtained simulating the three crimping procedures with the holding step (PH_{15}, PH_{30}, and PH_{60}) using all the developed PLLA elastic-viscous-plastic models, with detail of maximum force reached once the device is at the minimum diameter. The various simulations were labelled with the following strategy: the first letters refer to the crimping procedure (the presence of subscript numbers indicates a difference in step duration), then the temperature and the adopted material model are declared.

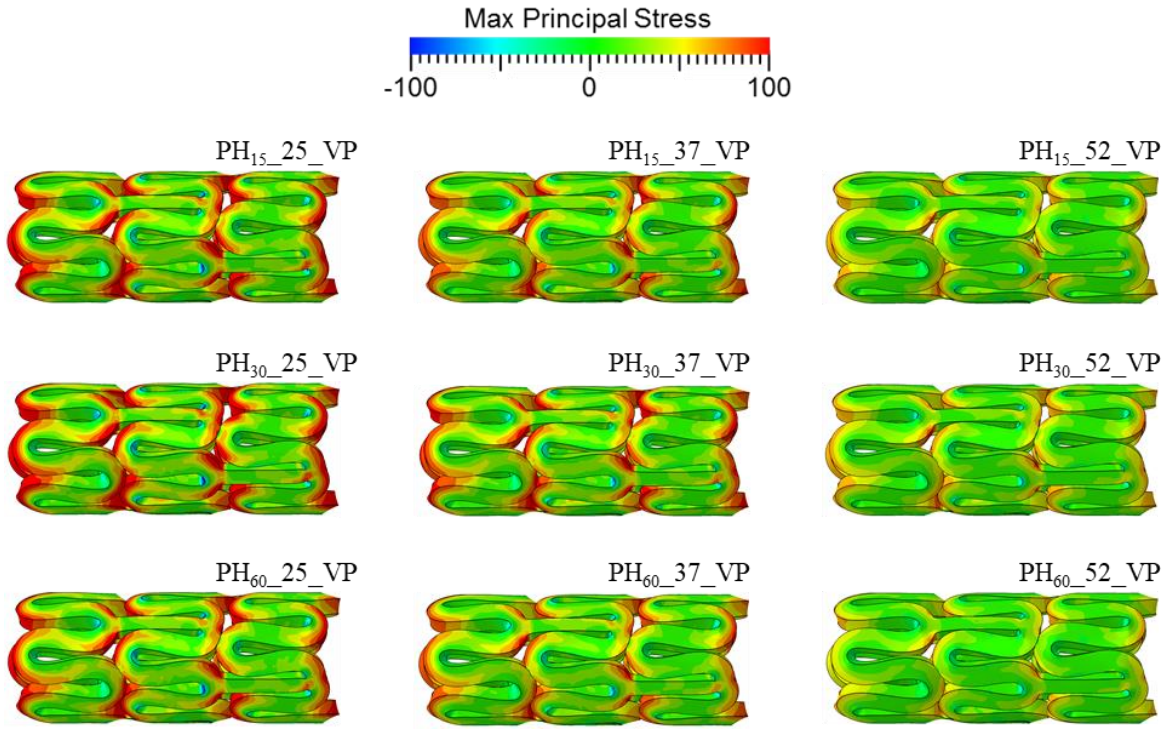

Figure 9 - Max Principal Stress recorded on the stent unit when the crimping planes reach the minimum diameter during the three crimping procedures with the holding step (PH_{15}, PH_{30}, and PH_{60}) for each elastic-viscous-plastic PLLA model. The various simulations were labelled with the following strategy: the first letters refer to the crimping procedure (the presence of subscript numbers indicates a difference in step duration), then the temperature and the adopted material model are declared.

The simulation outputs are reported also for the crimping procedure set according to the indications of Abbott's patent (PP) and the modified version with reduced target diameter (Modified_PP).

The final external diameter is equal to 1.506 mm and 1.380 mm respectively with protocol PP and Modified_PP, corresponding to an elastic recoil of 26.6% in both cases. These values are significantly lower than those obtained with the previously investigated crimping procedures. Although the complexity of procedure PP (performed at 52°C), the peak of crimping force recorded at the minimum crimped diameter is comparable with what was observed in PS and PH simulations carried out with the PLLA 52_VP model, indicating that this macroscopic quantity is not very sensitive to variations in the procedure as long as the minimum crimping diameter is maintained. On the other hand, such value significantly increased in the modified protocol, even if the minimum diameter reached at the end of the crimping phase was decreased by only 0.1 mm. In Figure 10 the stress states at the end of the crimping phase, after the crimping plan maintenance phase, and at the end of the plane reopening step are reported for the two simulations. The stress map clearly shows how the stent struts are affected by stress-relaxation during the maintenance step.

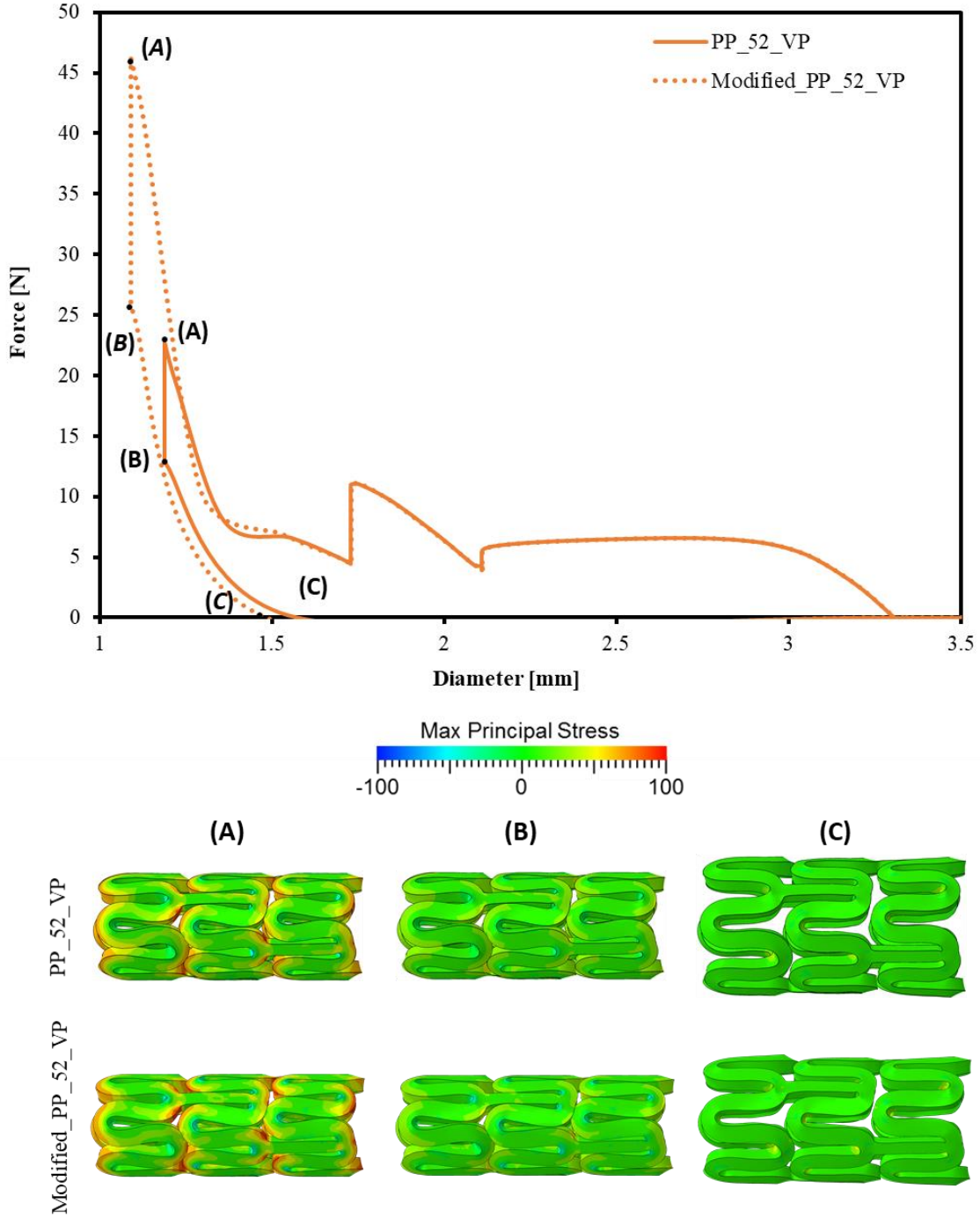

Figure 10 - Simulation results obtained carrying out the crimping procedure as stated by the stent manufacturer (PP) and with the modified procedure (Modified_PP) at 52°C. On the top, the force-diameter graph is shown, while, on the bottom, the stress status of the stent in three phases of the simulations is reported: (A) minimum crimping diameter, (B) end maintenance step, and (C) end of the procedure.

6. Discussion

The results of the experimental activity carried out on dog-bone specimens reflect what stated in the literature. The mechanical response of the PLLA is dependent on the operating temperature, while the viscous behavior is manifested mainly once the plastic deformations are reached since in the elastic field no significant changes were

appreciated as the test speed varied. The experimental protocol adopted for the tensile tests proved its efficacy in optimizing the number of information collected from a limited number of samples. Adding a long-lasting step for stress relaxation allowed gathering experimental data regarding the quasi-static mechanical behavior of the PLLA; this is a relevant characteristic to be evaluated when dealing with viscous structures subjected to bending, such as stents. Indeed, the presence of a neutral axis for bending implies that there is a portion of the stent strut with a null strain rate.

The material mechanical characteristics are describable with Johnson Cook's plasticity model, a simple and phenomenological material model already implemented in ABAQUS. The parameters, in the approximation, can be easily estimated from the experiments using the analytical expression of the relationship between stress and strain. In this work it was shown that the analytical method proved to be a simple and effective tool to obtain a model able to describe the viscous-plastic behavior of PLLA, although it is advisable to perform a subsequent optimization by replicating in-silico the experimental tests.

Due to the availability of a small number of PLLA specimens, it was not possible to perform a more in-depth experimental assessment of the risk of damage. The breakage of the specimens occurred in the tests carried out at 25°C (at both strain rates) and at 37°C with a strain rate equal to 10%/s, suggesting that the risk of polymer damage is strongly sensitive to test speed and operating temperature.

Consequently, the experimental evidence did not allow a survey of the rupture conditions as the strain rate and temperature of the stent varied. It was therefore not possible to establish a criterion for assessing in which procedure the stent would or would not fail. For this reason, this work was limited to a comparative analysis, assessing which crimping procedure is potentially more dangerous than others, but without identifying in which ones the device would break.

Comparing the results of the crimping simulations with simplified approach (PS) performed with the elastic-plastic and elastic-viscous-plastic material models, it can be seen that the choice to simplify the material model by neglecting the viscous effects of PLLA might result in an over/under-estimation (depending on the speed used to calibrate the elastic-plastic model) of the obtained diameter (Table 3) and the whole force-displacement curve (Figure 6). The elastic-plastic model calibrated on the tensile curves of the PLLA at 0.1%/s strain rate presented a lower elastic recoil than that obtained with the model tested at 10%/s. The differences were approximately equal to 4% at 37°C and reached a maximum value of 14% at 52°C. This difference was greater than the range found in the results of the simulations carried out considering viscous materials. The values of elastic recoil achieved with the PS_{30} and PS_{150} simulations differed by about 5% for all temperatures. This underlines the fact that an elastic-plastic model is unsuitable for this application, as it may lead to non-negligible errors in the diameter evaluation, especially if it is not known whether it is by excess or by defect with respect to the adopted crimping procedure.

Also, comparing the EP with VP materials, the analysis of the stresses reached at the minimum crimping diameter (Figure 7) showed that the approximation given by the elastic-plastic model lead to a too conservative assessment of the risk of device

damage. In fact, with the elastic-viscous-plastic model, the areas subjected to high stresses were less extensive. This difference is particularly evident considering the simulations related to 52°C.

Regarding the selection of an effective and safe crimping strategy, the comparison of the PS_{30} simulations performed with the elastic-viscous-plastic models with the procedures PH_{30} in which the minimum diameter was maintained fixed for 30 s before the reopening of the crimping planes, showed the beneficial effects of such a holding phase. Although the two procedures are equal in terms of minimum diameter reached during the crimping phase, the final diameters were smaller (with differences of about 6-7% in terms of elastic recoil) when a holding phase was performed. Therefore, the two procedures can be considered equivalent in terms of damage risk (same minimum diameter reached during crimping), but the one with the holding is to be preferred since allows achieving a finial configuration of the stent characterized by a lower diameter.

Intending to minimize the risk of damage during the crimping phase of the device, the maximum internal stress states detected with the PH_{15}, PH_{30} and PH_{60} procedures indicated that a crimping strategy involving crimping phases of long-time duration is advisable. For the same reason, a crimping procedure performed at elevated temperatures is to be preferred in any case, since in such condition, the polymer has a less rigid mechanical behavior, and consequently it is less subjected to the onset of stress peaks in the struts of the stent.

In the crimping procedure described in the Absorb stent patent, all these strategies were employed: the stent was subjected to temperatures higher than body temperature, the procedure took a long time and there were several steps in which the diameter was kept fixed to allow stress relaxation. This procedure was superior to the others described in this work: the stent at the end of the crimping process reached a smaller diameter without incurring high stresses during the loading history, thus maintaining reduced risks of damage to the structure.

The comparison of the two complex procedures (PP and Modified_PP) showed that the exclusive observation of macroscopic quantities such as the force-diameter relationship may be improper for evaluating the crimping procedure. In fact, it can be seen that the curve relative to the modified procedure (Modified_PP) presented a significantly higher force peak than that of the patent-inspired procedure (PP). This is due to a higher contact force between the stent struts caused by the reduction of the minimum diameter reached during the procedure. Taking into account only this information (that might be directly acquired during experimental crimping procedure) could lead to the hypothesis that the second procedure is significantly riskier for stent damage. Nevertheless, the analysis of the stress state inside the device showed that the two procedures were substantially equivalent in terms of damage risk while the percentage of diameter reduction with respect to the initial undeformed dimeter were equal to 54.6% and 58.4% respectively.

For a stent manufacturer, it is therefore fundamental to be able to develop an effective and safe crimping strategy and computational finite element simulations can provide a valid tool to evaluate the results of different procedures in terms of final reached diameters and internal stresses in the device, provided that the viscous and

temperature dependent mechanical characteristics of the polymer are considered in the adopted material model.

7. Acknowledgments

The authors acknowledge Giulia Bruno, Sara Colombo and Mattia Iaccheri for their technical support in the preliminary phase of the work.
This project has received funding from the European Union's Horizon 2020 research and innovation program under grant agreement n° 777119.
This article reflects only the authors' view and the Commission is not responsible for any use that may be made of the information it contains.

8. References

Bergström, J.S., Hayman, D., 2016. An Overview of Mechanical Properties and Material Modeling of Polylactide (PLA) for Medical Applications. Ann. Biomed. Eng. 44, 330–340. https://doi.org/10.1007/s10439-015-1455-8

Bergström, J.S., Kurtz, S.M., Rimnac, C.M., Edidin, A.A., 2002. Constitutive modeling of ultra-high molecular weight polyethylene under large-deformation and cyclic loading conditions. Biomaterials 23, 2329–2343. https://doi.org/10.1016/S0142-9612(01)00367-2

Blair, R.W., Dunne, N.J., Lennon, A.B., Menary, G.H., 2019. Characterisation and constitutive modelling of biaxially stretched poly(L-lactic acid)sheet for application in coronary stents. J. Mech. Behav. Biomed. Mater. 97, 346–354. https://doi.org/10.1016/j.jmbbm.2019.05.039

Bobel, A.C., McHugh, P.E., 2018. Computational Analysis of the Utilisation of the Shape Memory Effect and Balloon Expansion in Fully Polymeric Stent Deployment. Cardiovasc. Eng. Technol. 9, 60–72. https://doi.org/10.1007/s13239-017-0333-y

Bobel, A.C., Petisco, S., Sarasua, J.R., Wang, W., McHugh, P.E., 2015. Computational Bench Testing to Evaluate the Short-Term Mechanical Performance of a Polymeric Stent. Cardiovasc. Eng. Technol. 6, 519–532. https://doi.org/10.1007/s13239-015-0235-9

Cabrera, M.S., Oomens, C.W.J., Baaijens, F.P.T., 2017. Understanding the requirements of self-expandable stents for heart valve replacement: Radial force, hoop force and equilibrium. J. Mech. Behav. Biomed. Mater. 68, 252–264. https://doi.org/10.1016/j.jmbbm.2017.02.006

Debusschere, N., Segers, P., Dubruel, P., Verhegghe, B., De Beule, M., 2015. A finite element strategy to investigate the free expansion behaviour of a biodegradable polymeric stent. J. Biomech. 48, 2012–2018. https://doi.org/10.1016/j.jbiomech.2015.03.024

Eswaran, S.K., Kelley, J.A., Bergstrom, J.S., Giddings, V.L., 2011. Material Modeling of Polylactide. Simulia Cust. Conf. 1–11. https://doi.org/10.1007/978-3-642-45422-6_10

Jow, K.F., Yang, A.S., Wang, Y., Yan, K.W., 2012. Patent USOO8261423B2 Methods For Crimping a Polymeric Stent on to a Delivery Balloon 2.

Morris, P.D., Iqbal, J., Chiastra, C., Wu, W., Migliavacca, F., Gunn, J.P., 2018. Simultaneous kissing stents to treat unprotected left main stem coronary artery

bifurcation disease; stent expansion, vessel injury, hemodynamics, tissue healing, restenosis, and repeat revascularization. Catheter. Cardiovasc. Interv. 92, E381–E392. https://doi.org/10.1002/ccd.27640
Muliana, A., Rajagopal, K.R., 2012. Modeling the response of nonlinear viscoelastic biodegradable polymeric stents. Int. J. Solids Struct. 49, 989–1000. https://doi.org/10.1016/j.ijsolstr.2011.12.007
Pauck, R.G., Reddy, B.D., 2015. Computational analysis of the radial mechanical performance of PLLA coronary artery stents. Med. Eng. Phys. 37, 7–12. https://doi.org/10.1016/j.medengphy.2014.09.014
Qiu, T., He, R., Abunassar, C., Hossainy, S., Zhao, L.G., 2018. Effect of two-year degradation on mechanical interaction between a bioresorbable scaffold and blood vessel. J. Mech. Behav. Biomed. Mater. 78, 254–265. https://doi.org/10.1016/j.jmbbm.2017.11.031
Qiu, T.Y., Song, M., Zhao, L.G., 2018. A computational study of crimping and expansion of bioresorbable polymeric stents. Mech. Time-Dependent Mater. 22, 273–290. https://doi.org/10.1007/s11043-017-9371-y
Schiavone, A., Abunassar, C., Hossainy, S., Zhao, L.G., 2016. Computational analysis of mechanical stress–strain interaction of a bioresorbable scaffold with blood vessel. J. Biomech. 49, 2677–2683. https://doi.org/10.1016/j.jbiomech.2016.05.035
Schiavone, A., Qiu, T.-Y., Zhao, L.-G., 2017. Crimping and deployment of metallic and polymeric stents -- finite element modelling. Vessel Plus 1, 1–10. https://doi.org/10.20517/2574-1209.2016.03
Soares, J.S., Moore, J.E., Rajagopal, K.R., 2010. Modeling of deformation-accelerated breakdown of polylactic acid biodegradable stents. J. Med. Devices, Trans. ASME 4. https://doi.org/10.1115/1.4002759
Wang, P.J., Berti, F., Antonini, L., Nezami, F.R., Petrini, L., Migliavacca, F., Edelman, E.R., 2020. Multimodal Loading Environment Predicts Bioresorbable Vascular Scaffolds' Durability. Ann. Biomed. Eng. https://doi.org/10.1007/s10439-020-02673-z
Wang, Q., Fang, G., Zhao, Y., Wang, G., Cai, T., 2017. Computational and experimental investigation into mechanical performances of Poly-L-Lactide Acid (PLLA) coronary stents. J. Mech. Behav. Biomed. Mater. 65, 415–427. https://doi.org/10.1016/j.jmbbm.2016.08.033